ASTFE
American Society
of Thermal and Fluids Engineers

9th Thermal and Fluids Engineering Conference (TFEC)

April 21-24, 2024

Partially Online Virtual and at Oregon State University, OR Conference

TFEC-2024-xxxxx

OPPORTUNITIES FOR USING NUCLEAR MICROREACTORS FOR WASTEWATER TREATMENT, HYDROGEN PRODUCTION, AND AMMONIA PRODUCTION

Bailey Strine, Jack Pakkebier*, Prathap Parameswaran, Melanie M. Derby

Alan C. Levin Department of Mechanical and Nuclear Engineering, Carl R. Ice College of Engineering, Kansas State University, Manhattan, Kansas 66506, USA

ABSTRACT

In 2021, the White House proposed a 50-52% reduction in greenhouse gas emissions by the year 2030; therefore, there is significant interest in energy sources and processes that reduce carbon dioxide emissions. This paper presents a sensitivity analysis of a nuclear microreactor-powered design for concurrent hydrogen (H_2) and ammonia (NH_3) production, with a focus on wastewater treatment plant applications. Wastewater with organic materials (e.g., municipal wastewater, swine lagoon waste, and food waste) are the analyzed feedstocks. The system integrates the anaerobic digestion of wastewater sludge with a Brayton cycle-based power generation unit heated by the microreactor. Using empirical data and an analytical model, the paper investigates the system's response to variations in key operational parameters. The sensitivity analysis explores the influence of parameters such as the chemical oxygen demand of the feedstock, compressor isentropic efficiency, and reactor temperature and pressure on H_2 and NH_3 production rates, Brayton cycle efficiency, and carbon dioxide emissions. Highlights from this analysis show a nonlinear dependence for Brayton efficiency on reactor temperature, the proportionality of ammonia and hydrogen production on chemical oxygen demand values, the major impact of compressor isentropic efficiency, and the minimal response from changing the pressure of steam methane reforming. These results signify opportunities to improve the system and ultimately lead to lowered greenhouse gas emissions.

KEY WORDS: carbon neutral, nuclear microreactors, carbon dioxide emissions

1. INTRODUCTION

Reducing greenhouse gas emissions is of global importance. As atmospheric concentrations of greenhouse gases such as carbon dioxide (CO_2), methane (CH_4), and nitrous oxide (N_2O) have increased considerably over the last few centuries, the United States, the European Union, and China have targeted to reduce global emissions significantly by 2030 [1]–[4]. One opportunity is to incorporate carbon-neutral power sources in industrial processes to reduce carbon dioxide emissions [5], [6]. Hydrogen is currently used in making fertilizer, hydrogenating oils, hydrotreating, and as a sustainable fuel source [5], [7], [8]. Hydrogen can be synthesized through multiple processes such as steam methane reforming, electrolysis of water, and thermochemical water splitting [7]. Steam methane reforming produces 80-90% of hydrogen globally, but state-of-the-art steam methane reforming facilities produce 8.3 kg CO_2/ kg H_2 [9]. Ammonia is primarily produced for use as a fertilizer, which can enable a 30-50% increase in crop production [10]. Ammonia production via the Haber-Bosch process accounts for 1-1.2% of global greenhouse gas emissions [11], [12]. Some routes to reduce CO_2 emissions associated with hydrogen and ammonia production involve changing the methane source for steam methane reforming from natural gas to a biogas source, or by changing the

*Corresponding Author: jpakkebier@ksu.edu

hydrogen production method to allow for the use of other carbon-neutral hydrogen feedstocks. An example system for the production of biogas is an anaerobic membrane bioreactor (AnMBR). An AnMBR is a closed anaerobic digestion system that allows for the treatment of wastewater, capture of methane, and retention of the microbial community that breaks down organic material [13], [14]. Methane from an AnMBR is carbon neutral as the reactor is capturing methane that would leach into the atmosphere if the wastewater were stored in an uncovered lagoon, which is a conventional disposal method [15]. Anaerobic digestion is a biological process where anaerobic consortia including methanogenic archaea convert organic waste into carbon dioxide and methane [16]. This methane can then be used to supplement a power cycle as a heat source when in its biogas form and can also act as a feedstock for hydrogen production via steam methane reforming. Another promising avenue is the use of nuclear power plants and microreactors which produce electricity and heat. Using nuclear heat for steam methane reforming can decrease carbon dioxide emissions by 32.5% [5], [6]. This heat can also be diversified to power processes including hydrogen and ammonia production [17], [18].

The system proposed in this paper utilizes the excess heat from a nuclear microreactor to produce methane from an AnMBR, hydrogen via steam methane reforming, and ammonia via the Haber Bosch process. The ammonia production cycle is built around a nitrogen Brayton cycle which will also power the steam methane reformer and the AnMBR. This Brayton cycle includes an intermediate heat exchanger that supplies heat to the cycle, a gas turbine, a recuperator, a pre-cooler, a low-pressure turbine, an inter-cooler, and a high-pressure turbine that produces electricity at 40% thermal efficiency. The research objectives of this paper are to understand how the model responds to changes in key parameters such as chemical oxygen demand (COD) values of the feedstock used in the AnMBR, temperature leaving the intermediate heat exchanger, compressor isentropic efficiency, and pressure values such as the Brayton cycle pressure ratio and the pressure of steam methane reforming. Insight into how these changes impact performance metrics such as Brayton cycle efficiency, ammonia and hydrogen production, and CO_2 emissions are investigated.

2. MODEL

The microreactor used as a reference in this study is the U-battery manufactured by Urenco, which is helium-cooled and produces heat at 983 K [19]. The Brayton cycle (Figure 1), connected to the microreactor via an intermediate heat exchanger, uses nitrogen as the working fluid with a Brayton cycle efficiency of 40%. An Engineering Equation Solver (EES) program is written based on this Brayton cycle to determine the turbine pressure ratio, turbine efficiency, compressor efficiency, and recuperator effectiveness needed to match the cycle efficiency reported by Urenco for the Brayton cycle efficiency of 40%. This code is the framework for the model which co-generates hydrogen and ammonia.

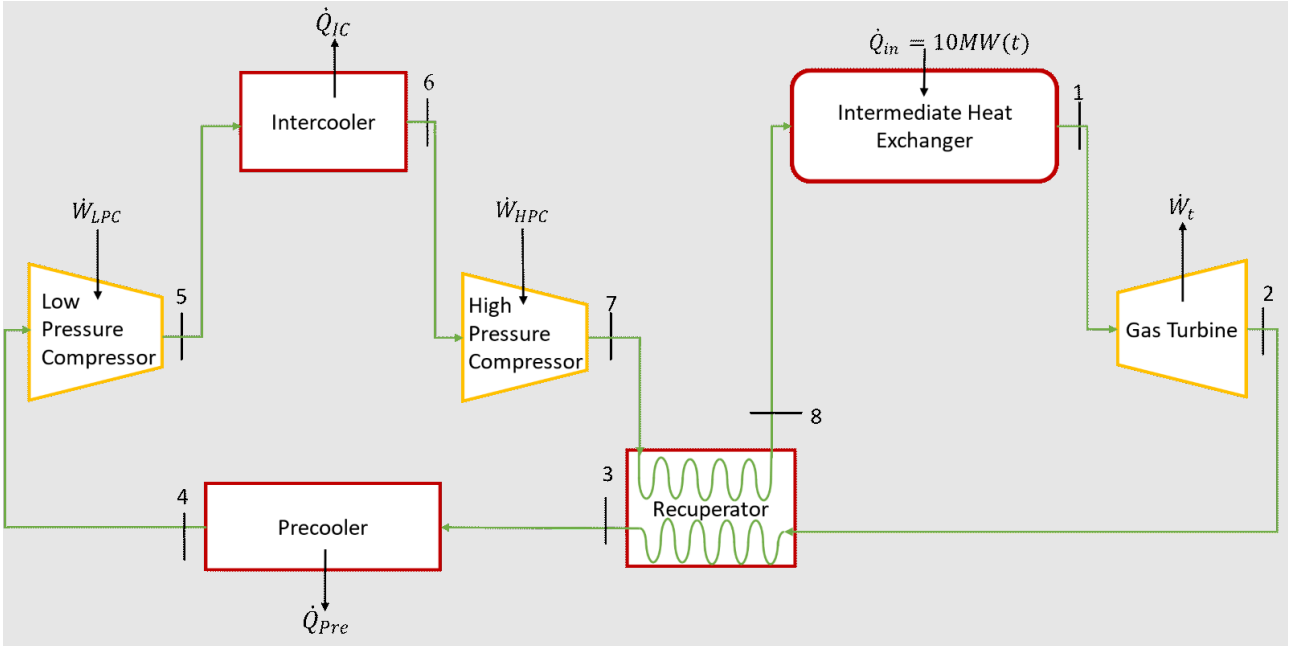

Figure 1: Brayton cycle powered by 10 MW(t) heat from nuclear microreactor.

The working fluid in the Brayton cycle loop is nitrogen as a real gas. The pressure needed for the heat loop in nuclear steam methane reforming is 4 MPa [20] which is set for state 1. For state 4, the temperature is set to ambient (301 K). Then, for the lowest compressor work using intercooling, the temperature at state 6 equals the temperature of state 4 [21]. For this thermodynamic model, it is also assumed that through all the heat exchangers there is a zero pressure drop and the pressure ratios of the low-pressure and high-pressure compressors are equal. After the turbine for state 2, the temperature is calculated using the isentropic turbine efficiency (set to 92%) and the pr92essure ratio, which is varied (Eq. 1-3). All of the equations used for the calculations regarding this system can be seen in Figure A in the appendix. The compressor pressure ratio is utilized to find the pressure of state 5 (Eq. 4). Using this pressure, the enthalpy of state 5 is set using the isentropic efficiency of the compressor (set to 80%). Similarly, the enthalpy and temperature of state 7 is set using the compressor isentropic efficiency (Eq. 5, 6). Next, for state 8, the temperature is determined using the heat provided by the intermediate heat exchanger, the nitrogen flow rate, and the enthalpy at state 1. The enthalpy for state 8 can be determined, and using EES, the temperature of state 8 at the specified pressure and enthalpy is interpolated (Eq. 7). To finish the Brayton cycle analysis, state 3 is set by using the effectiveness of the recuperator (Eq. 8). All of the states, variables, and their numerical values can be seen in Table 1.

Table 1. States set for Brayton cycle model.

State	Property	Property	Description
1	P = 4 MPa [20]	T = 983 K [19]	[19], [20]
2	P = 1.27 MPa	H = 22095 kJ/kmol	$\eta_t = 92\%$, Eq. 1-3
3	P = 1.27 MPa	H = 12064 kJ/kmol	Eq. 1, 8
4	P = 1.27 MPa	T = 301 K	Ambient temperature, Eq. 1
5	P = 2.26 MPa	H = 10623 kJ/kmol	$\eta_c = 80\%$, Eq. 4
6	P = 2.26 MPa	T = 301 K [21]	Assume no pressure drop, [21]
7	P = 4 MPa	H = 10568 kJ/kmol	$\eta_c = 80\%$, Eq. 5, 6
8	P = 4 MPa	H = 20577 kJ/kmol	Eq. 7

Subsequently, the model is expanded to include hydrogen and ammonia production (Figure 2). The nuclear microreactor provides 10 MW of heat to the cogeneration cycle through an intermediate heat exchanger which powers the Brayton cycle, a steam methane reformer to produce H_2, and a Haber-Bosch reactor to produce NH_3. The steam methane reformer is added before the gas turbine due to its requirements for the highest operating temperature in the process, 723 K. The steam methane reformer takes steam produced by adding a feedwater heater and heat recovery steam generator to the nitrogen heat loop and takes methane produced by the AnMBR. The AnMBR requires a wastewater source, ultrafiltration membrane modules along with permeate and recirculation pumps, pressure swing adsorption (PSA) unit for biogas purification, and a methane compressor to produce methane. The PSA unit is needed to purify the methane produced by the AnMBR and delivers methane at 85-98% purity [9], [22]–[26]. To enhance the hydrogen production rate within the system, a water-gas shift (WGS) reactor is incorporated into the process. Additionally, a heat exchanger is introduced to cool down the reactants before they enter the WGS reactor. This heat exchanger serves a dual purpose: it warms the nitrogen required for ammonia production, which is generated through air separation using a PSA unit. The nitrogen is subsequently heated and pressurized before being introduced into the Haber-Bosch reactor. The hydrogen produced in the steam methane reformer and the WGS reactor is combined and compressed before being fed into the Haber-Bosch reactor. The condenser is employed to separate the ammonia from the hydrogen and nitrogen left in the product stream of the Haber-Bosch reactor.

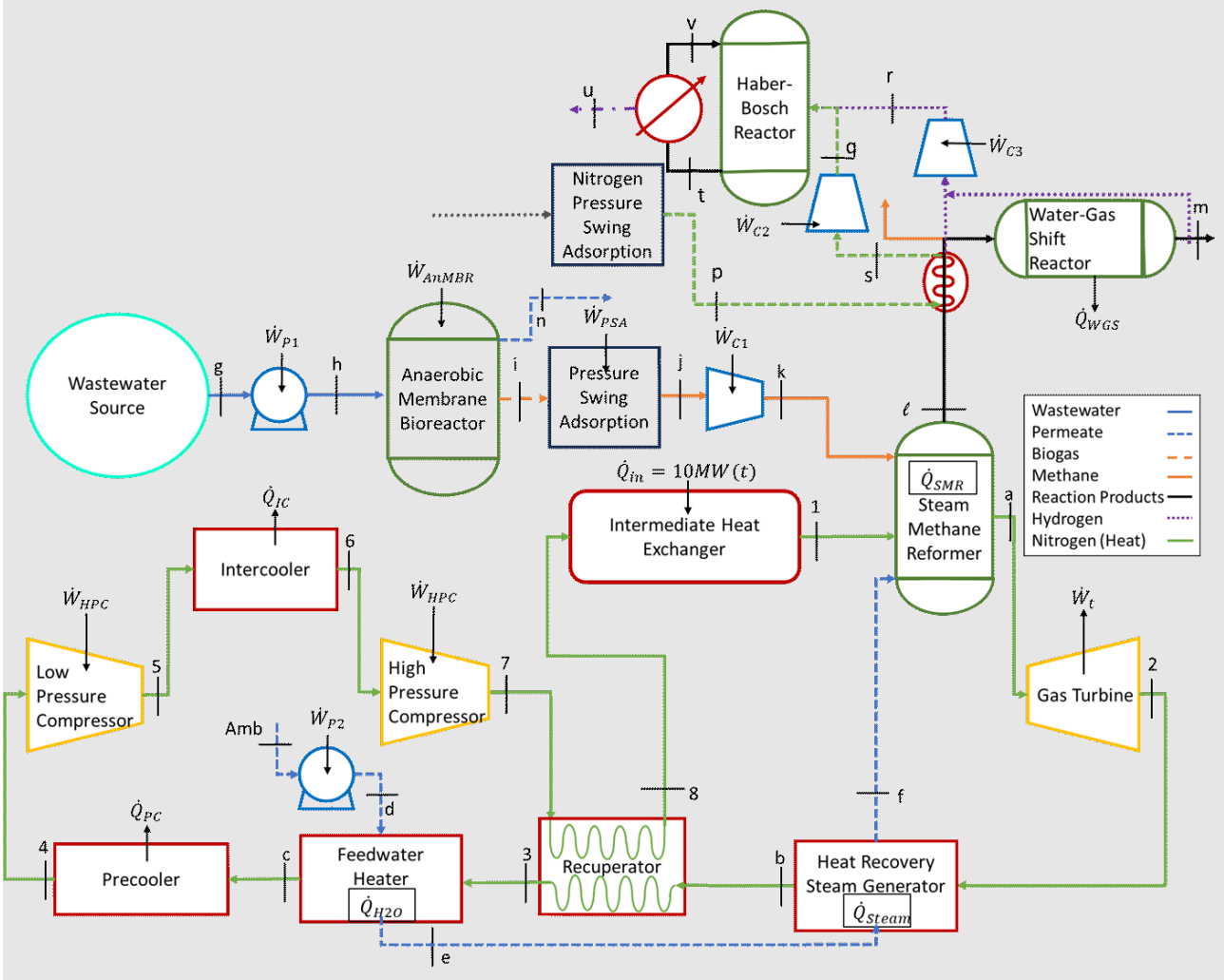

Figure 2: Schematic of proposed wastewater treatment and hydrogen/ammonia production cycle built from the nitrogen Brayton cycle.

The symbols used in Figure 5.2 are: $\dot{Q}$ is heat in kW, $\dot{W}$ is work in kW, $\dot{n}$ is the flow rate in kmol/s, H is enthalpy in kJ/kmol, ε is effectiveness, and η is efficiency. Subscripts are used to determine which unit process the equation is referring to: SMR for steam methane reformer, T for turbine, HRSG for heat recovery steam generator, REC for recuperator, FW for feedwater heater, PC for precooler, LPC for low-pressure compressor, C for compressor, IC for intercooler, and HPC for high-pressure compressor.

3. SENSITIVITY ANALYSIS

A sensitivity analysis was conducted on the cycle to determine how certain parameters impact key characteristics of the system such as H_2 and NH_3 production rates, Brayton cycle efficiency, and carbon dioxide emissions. The sensitivity analysis was conducted using EES, where parametric tables were employed to vary parameters. The parameters considered for this sensitivity analysis are the COD of the incoming permeate feedstock, temperatures and pressures of critical components, the Brayton cycle pressure ratio, and the isentropic efficiency of the low- and high-pressure compressors. The anaerobic wastewater treatment produces a varying amount of methane depending on the feedstock. There are many different kinds of feedstocks, but this study focuses on three in particular, food waste, swine, and municipal wastewater. These three feedstocks vary in methane production due to differences in their COD. The municipal wastewater COD information is based on primary data from a pilot scale AnMBR on Kansas State University's campus provided by Dr. Prathap Parameswaran [27]. The COD data for swine wastewater was determined by Tang et. al [28] and the COD data for the food wastewater stream was determined by Cheng et. al [14] and Cheng et. al [29].

Table 2: COD values for municipal, swine, and food waste wastewater streams.

Feedstock	gCOD/L	L CH_4/gCOD
Municipal	0.316-1.79	0.125
Swine	15-35	0.24
Food Waste	44.4-82.1	0.22-0.31

As shown in Figure 3, when the wastewater treatment rate is held constant at 74,000 gallons/day for each feedstock, the wastewater feedstock with the highest hydrogen and ammonia production is food waste followed by swine and then municipal. This result highlights the difference that COD values in a feedstock make on hydrogen and ammonia production.

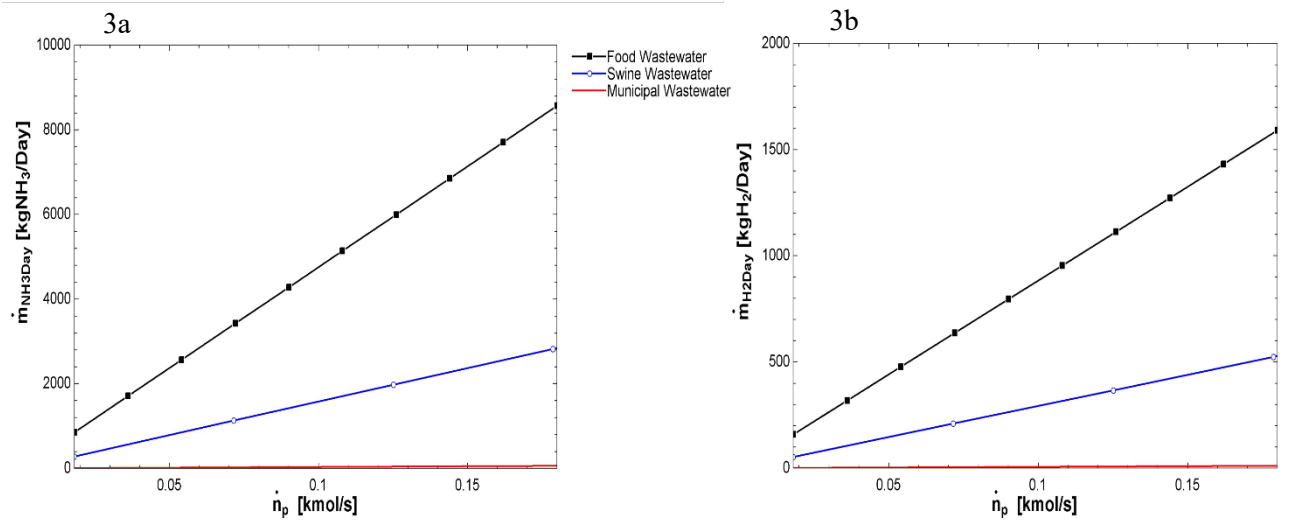

Figure 3: (3a) The ammonia production in kg/day vs. permeate flowrate plotted for each feedstock. (3b) The hydrogen production in kg/day vs. permeate flowrate plotted for each feedstock.

Beginning the sensitivity analysis and knowing the effect of COD on hydrogen and ammonia production, the parameter changed in EES was the gCOD/L permeate, which is grams of COD per liter of the incoming permeate. For each feedstock we investigated, the effect of gCOD/L permeate on daily ammonia and hydrogen production using the range of values shown in Table 2. In each case considered, the ammonia and hydrogen production corresponded proportionally to the change in gCOD/L permeate. This makes sense as the equations used to calculate the daily ammonia and hydrogen production are linear functions of methane production (Eq. 9). For each feedstock, the gCOD/L permeate was monitored over the range shown in Table 2. As a result, ammonia and hydrogen production responded proportionally. An example to show the linear effect of gCOD/L permeate variance on daily ammonia and hydrogen production can be seen in Figure 4a where the municipal wastewater case was analyzed. Units of gCOD/L permeate were changed to gCOD/kmol H_2O for ease of calculation.

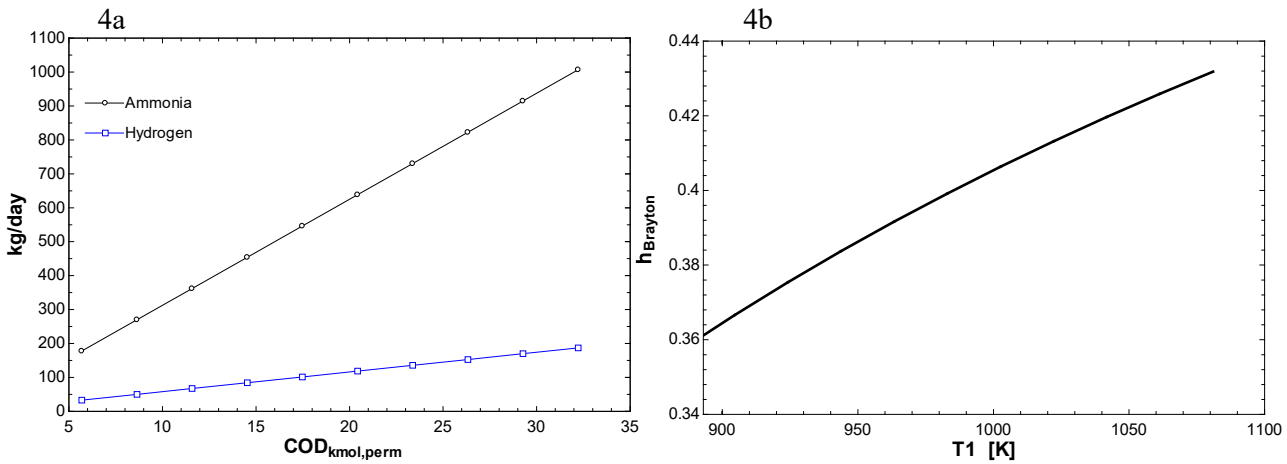

Figure 4: (4a) Ammonia and hydrogen daily production vs. gCOD/kmol H_2O for municipal wastewater. (4b) Brayton efficiency versus state 1 temperature.

Changing the gCOD/L of permeate also affects the carbon dioxide emissions from the system. As shown in Figure 5, each feedstock was analyzed over the range of gCOD/L values from Table 2. Increasing the gCOD/L permeate for each feedstock resulted in higher total carbon dioxide emissions. The municipal wastewater stream has by far the lowest carbon dioxide emissions, followed by swine wastewater and then food wastewater. It is important to note that even though the municipal wastewater stream had the lowest carbon dioxide emissions, it also had significantly lower ammonia and hydrogen production rates compared to the other two studied streams in this paper. The carbon dioxide emissions ratio for hydrogen production from this cycle is 5.74 $kgCO_2/kgH_2$. A state-of-the-art nuclear steam methane reforming plant produced carbon dioxide at the rate of 5.6 $kgCO_2/kgH_2$ [5], showing that this cycle produces carbon dioxide emissions at roughly the same rate as a state-of-the-art plant. The carbon dioxide emissions rate for ammonia produced using hydrogen from steam methane reforming is 1.5-1.6 kg CO_2/kg NH_2 [10], [11]. This cycle has a lower emissions rate of 1.07 kgCO2/kgNH3 for the ammonia produced using hydrogen from nuclear steam methane reforming. Since the carbon dioxide emissions are a function of how much hydrogen and ammonia are produced, it makes sense that the feedstock with the highest production of ammonia and hydrogen also has the highest production rate of CO_2.

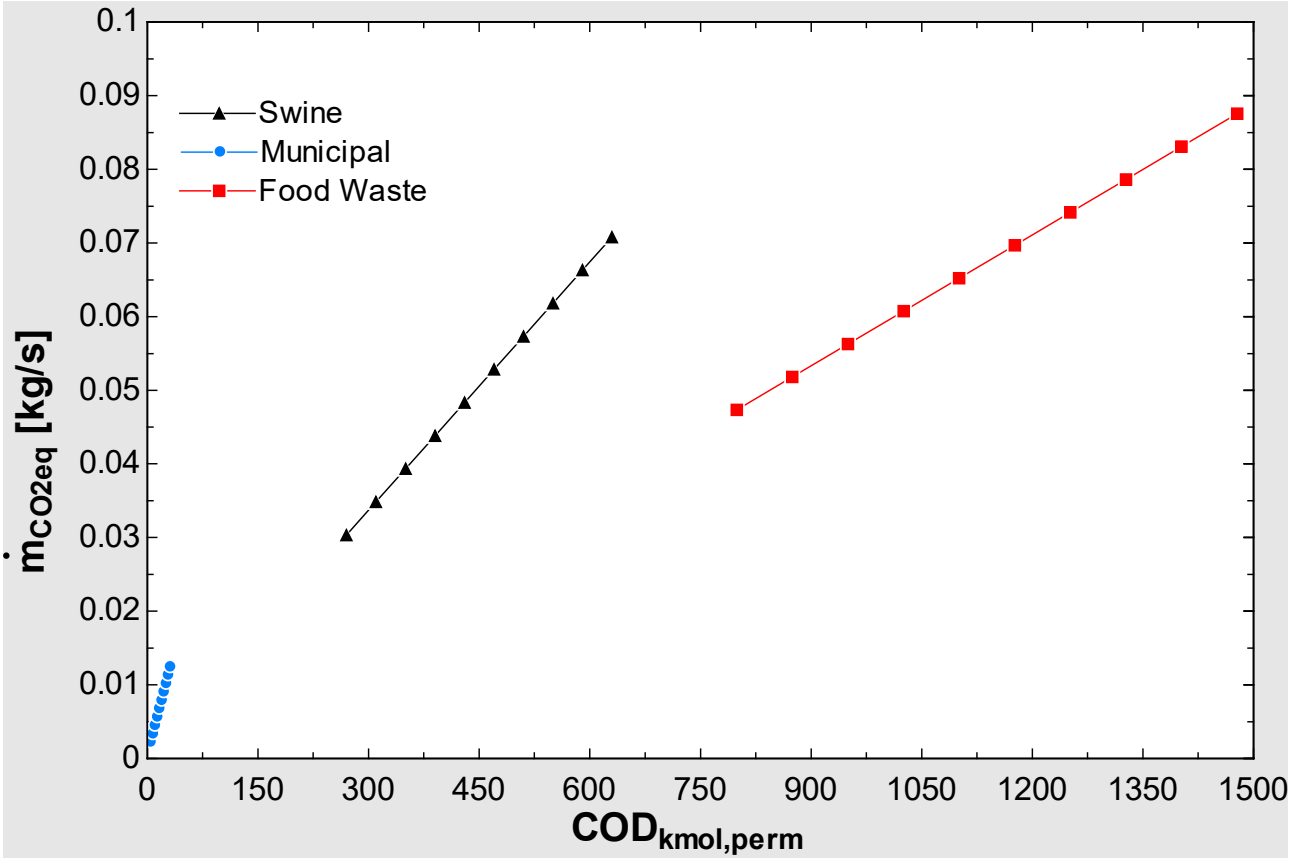

Figure 5: CO_2 equivalent mass flow rate (kg/s) versus gCOD/kmol H_2O for each feedstock considered.

The next parameters considered in the sensitivity analysis are the temperatures and pressures of critical components in the system. Since this system is modeled after Urenco's U-Battery, the temperature leaving the intermediate heat exchanger, state 1, is set at 983 K. To see how sensitive the system is to variance in this temperature, the system was run at a temperature range of 885-1081 K (plus and minus 10% of 983 K). This change led to a noticeable response in the Brayton cycle efficiency, $\eta_{Brayton}$, depicted in Figure 4b. Increasing the temperature by 10% up to 1081 K led to a 43.2% Brayton efficiency, up 3.3% from the base 40% the cycle currently runs at. However, decreasing the state 1 temperature by 10% down to 885 K resulted in a Brayton efficiency of 35.8%, 4.2% down from the base 40%, suggesting that there is some nonlinearity in the system.

Now, when considering the pressure values in the system, two values were analyzed; the pressure ratio used in the Brayton cycle and the pressure of the SMR. The current pressure ratio used for the cycle is 3.14 across the gas turbine (Eq. 4). This pressure ratio value will bring the Brayton efficiency of the cycle to 40% when coupled with the microreactor. Using a similar approach as done earlier, the pressure ratio was varied from a much lower value to a much higher value to see how the system responds. The pressure ratio was plotted from 1-15 to see the effects on the Brayton efficiency, which can be seen in Figure 6. From the plot, the ideal pressure ratio is 3.22. However, both the current value of 3.14 and the max value of 3.22 closely round to 40% efficiency and are practically identical. The peak performance of the system is indicated with a red triangle in Figure 4a. As the pressure ratio is increased further, the Brayton efficiency gradually declines. Meanwhile, as the pressure ratio is decreased to 1, the Brayton efficiency tends to 0% as it will be impossible for the turbine to do work.

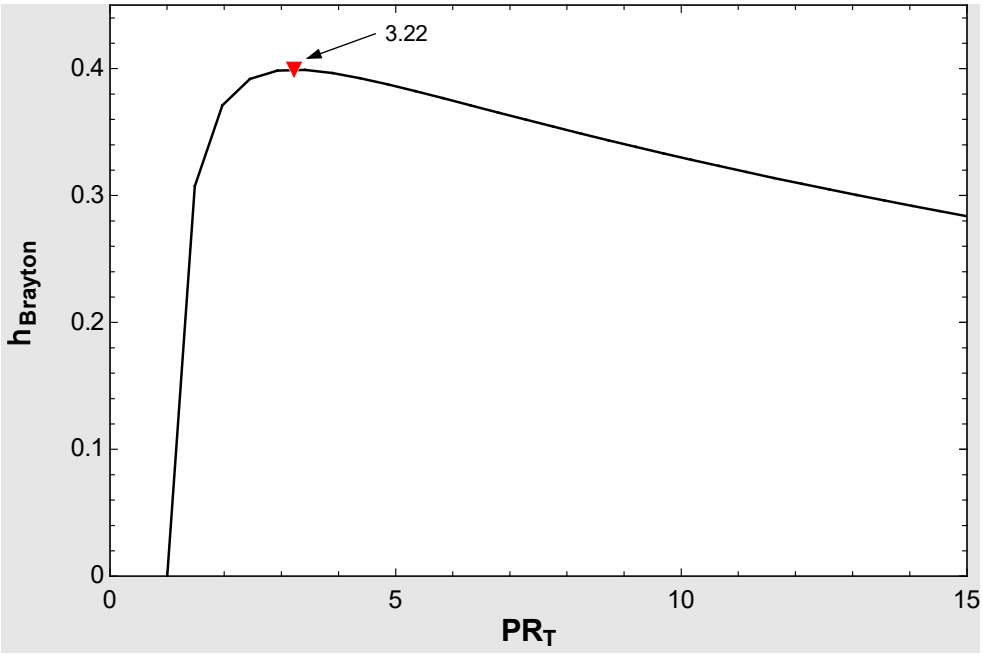

Figure 6: Brayton efficiency plotted against turbine pressure ratio, PR_T. A red triangle is placed to indicate the pressure ratio with the highest Brayton efficiency, 3.22.

Since the pressure needed for the heat loop in steam methane reforming is 4 MPa [20], the outcome of changing this pressure is sought out. Steam methane reforming can often have a reaction pressure of 0.5-10 MPa [30]–[32]. This range is used in this analysis to investigate the effects of steam methane operating pressures in the cycle. Simply put, in our system, the variance in SMR pressure has little effect on cycle characteristics. The only observed change was in the Brayton cycle efficiency, where the effects were extremely limited. In the analysis, running from 0.5 MPa to 10 MPa only resulted in a 0.5% increase in the Brayton efficiency.

The final parameter considered is the isentropic efficiency of the low- and high-pressure compressors utilized in the system. Currently, it is assumed that these compressors each have an isentropic efficiency of 80%. As one would expect, variance in this parameter had large effects on the efficiency of the system. For the sensitivity analysis, the range considered for changing this parameter is 60-90%. When the compressor isentropic efficiency is lowered to 60%, the Brayton efficiency drops significantly, dropping down to 25.8%. Likewise, when the compressor isentropic efficiency is raised to 90%, the Brayton efficiency increases to 44.6%, as shown in Figure 7.

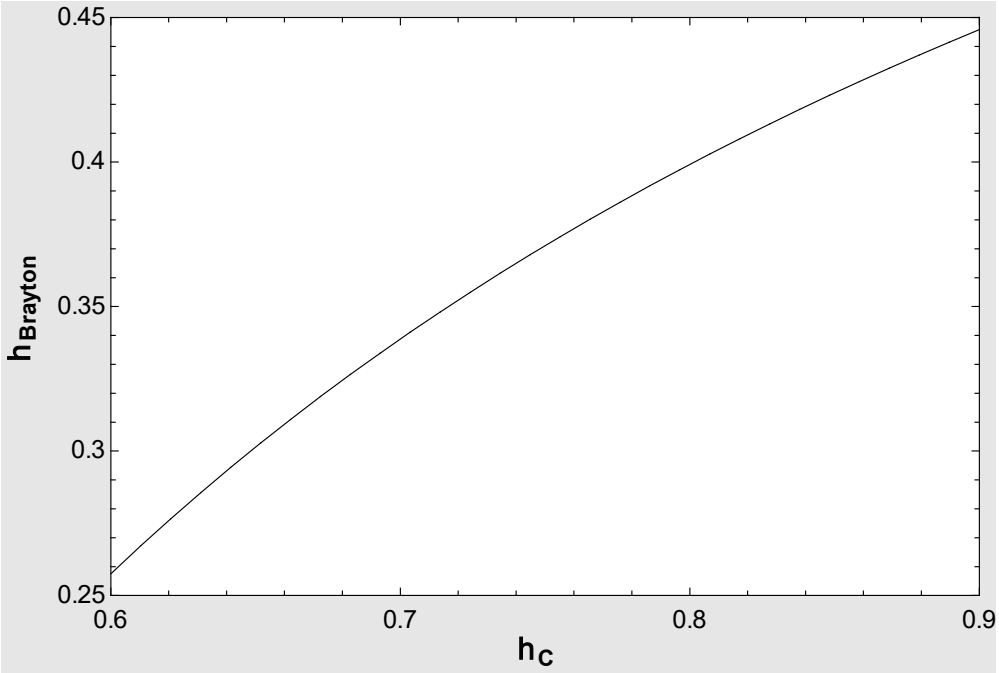

Figure 7: Brayton efficiency plotted against isentropic compressor efficiency.

With the initial purchase of a more expensive, higher-efficiency compressor, the 4.6% increase in Brayton efficiency would certainly pay for itself throughout operation. The lower compressor isentropic efficiency indicates greater energy loss throughout the compression process and it is clear that a higher efficiency value is generally desirable. The system also currently operates with an assumed turbine isentropic efficiency of 92%. The same principles apply to the turbine isentropic efficiency like the compressor isentropic efficiency. 92% is already a competitively high rating, making decreases in this efficiency unwanted.

4. CONCLUSIONS

This study explored the sensitivity of a nuclear microreactor-powered design for concurrent hydrogen and ammonia production, with a focus on wastewater treatment applications. The findings from this analysis include the proportionality between variance in chemical oxygen demand (COD) and ammonia and hydrogen production rates. Along with variance in COD values, higher COD values resulted in increased carbon dioxide emissions, showing the need for balance when considering production rates with emissions reductions. The response due to changing the temperature entering the steam methane reformer was nonlinear and resulted in a noticeable influence on Brayton efficiency. When temperature was changed from the base 983 K to 1081 K (a 10% increase), the Brayton efficiency improved by 3.3% and when lowered from 983 K to 885 K (a 10% decrease), the Brayton efficiency decreased by 4.2%. The optimal pressure ratio for the Brayton cycle was found to be 3.22, where deviance in this value only resulted in decreased efficiencies. Also, the pressure at which steam methane reforming takes place was investigated but changing this pressure value seemed to have a very minimal effect on any output studied. Lastly, the compressor isentropic efficiency was shown to have a significant influence on Brayton cycle efficiency, as expected. Improvements in compressor technology directly led to better overall efficiencies. This nuclear microreactor-based approach shows promise for efficient and carbon-neutral wastewater treatment, hydrogen production, and ammonia production, aligning with emission reduction goals.

5. APPENDIX

$$PR_T = \frac{P_1}{P_2} \quad (1)$$

$$\eta_T = \frac{H_1 - H_2}{H_1 - H_{2s}} \quad (2)$$

$$\dot{W}_T = \dot{n}_{N2}\eta_T(H_1 - H_2) \quad (3)$$

$$PR_{HPC}\ x\ PR_{LPC} = PR_C = PR_T \quad (4)$$

$$\eta_C = \frac{H_{5s} - H_4}{H_5 - H_4} \quad (5)$$

$$\dot{W}_{LPC} = \frac{\dot{n}_{N2}(H_4 - H_5)}{\eta_C} \quad (6)$$

$$10{,}000\ kW = \dot{n}_{N2}(H_1 - H_8) \quad (7)$$

$$\varepsilon_{rec} = \frac{H_8 - H_7}{H_3 - H_7} \quad (8)$$

$$\dot{m}_p \left(\frac{gCOD}{L_{permeate}}\right)\left(\frac{LCH_4}{gCOD}\right) = \dot{m}_{CH_4} \quad (9)$$

Figure A: Equations referenced.

In Figure A, the variables are defined as follows: PR_T is the pressure ratio across the turbine, P_1 is the pressure at state 1, η_T is the isentropic turbine efficiency, H_1 is the enthalpy at state 1, H_{2s} is the isentropic enthalpy at state 2, $\dot{W}_T$ is the work of the turbine, $\dot{n}_{N2}$ is the molar flowrate of nitrogen, PR_{HPC} is the pressure ratio across the high-pressure compressor, PR_{LPC} is the pressure ratio across the low-pressure compressor, PR_C is the product of the compressor pressure ratios, η_C is the compressor isentropic efficiency, $\dot{W}_{LPC}$ is the work of the low-pressure compressor, ε_{rec} is the recuperator effectiveness, $\dot{m}_p$ is the mass flowrate of permeate, and $\dot{m}_{CH_4}$ is the mass flowrate of methane extracted from the wastewater.

ACKNOWLEDGMENTS

This work was supported by the Department of Energy Nuclear Energy University Programs under grant no. DE-NE0009152 and the National Science Foundation under grant no. 1828571.

REFERENCES

[1] V. Masson-Delmotte *et al.*, "Climate change 2021: the physical science basis," *Contribution of working group I to the sixth assessment report of the intergovernmental panel on climate change*, vol. 2, p. 24, 2021.

[2] "FACT SHEET: President Biden Sets 2030 Greenhouse Gas Pollution Reduction Target Aimed at Creating Good-Paying Union Jobs and Securing U.S. Leadership on Clean Energy Technologies," whitehouse.gov.

[3] "Total greenhouse gas emission trends and projections in Europe - 8th EAP," https://www.eea.europa.eu/ims/total-greenhouse-gas-emission-trends.

[4] "ACTION PLAN FOR CARBON DIOXIDE PEAKING BEFORE 2030," https://en.ndrc.gov.cn/policies/202110/t20211027_1301020.html.

[5] P. Sun and A. Elgowainy, "Updates of hydrogen production from SMR process in GREET® 2019," *Argonne National Laboratory: Lemont, IL, USA*, 2019.

[6] L. Hoseinzade and T. A. Adams II, "Modeling and simulation of an integrated steam reforming and nuclear heat system," *Int J Hydrogen Energy*, vol. 42, no. 39, pp. 25048–25062, 2017.

[7] J. D. Holladay, J. Hu, D. L. King, and Y. Wang, "An overview of hydrogen production technologies," *Catal Today*, vol. 139, no. 4, pp. 244–260, 2009.

[8] P. Sun *et al.*, "Criteria air pollutants and greenhouse gas emissions from hydrogen production in US steam methane reforming facilities," *Environ Sci Technol*, vol. 53, no. 12, pp. 7103–7113, 2019.

[9] D. Bonaquist, "Analysis of CO2 emissions, reductions, and capture for large-scale hydrogen production plants," http://www. praxair. ca/praxair. nsf/0/6D73B5DA741457DA8525772900703E30/$ file/Praxair-CO2EmissionsReductionCapture-WhitePaper.

[10] P. H. Pfromm, "Towards sustainable agriculture: Fossil-free ammonia," *Journal of Renewable and Sustainable Energy*, vol. 9, no. 3, 2017.

[11] C. Smith, A. K. Hill, and L. Torrente-Murciano, "Current and future role of Haber–Bosch ammonia in a carbon-free energy landscape," *Energy Environ Sci*, vol. 13, no. 2, pp. 331–344, 2020.

[12] Y. Bicer and I. Dincer, "Life cycle assessment of nuclear-based hydrogen and ammonia production options: A comparative evaluation," *Int J Hydrogen Energy*, vol. 42, no. 33, pp. 21559–21570, 2017.

[13] B.-Q. Liao, J. T. Kraemer, and D. M. Bagley, "Anaerobic membrane bioreactors: applications and research directions," *Crit Rev Environ Sci Technol*, vol. 36, no. 6, pp. 489–530, 2006.

[14] H. Cheng, Y. Li, L. Li, R. Chen, and Y.-Y. Li, "Long-term operation performance and fouling behavior of a high-solid anaerobic membrane bioreactor in treating food waste," *Chemical engineering journal*, vol. 394, p. 124918, 2020.

[15] D. C. Stuckey, "Recent developments in anaerobic membrane reactors," *Bioresour Technol*, vol. 122, pp. 137–148, 2012.

[16] M. Pecchi and M. Baratieri, "Coupling anaerobic digestion with gasification, pyrolysis or hydrothermal carbonization: a review," *Renewable and Sustainable Energy Reviews*, vol. 105, pp. 462–475, 2019.

[17] X. Yao, Y. Zhang, L. Du, J. Liu, and J. Yao, "Review of the applications of microreactors," *Renewable and sustainable energy reviews*, vol. 47, pp. 519–539, 2015.

[18] A. E. Karaca, I. Dincer, and J. Gu, "A comparative life cycle assessment on nuclear-based clean ammonia synthesis methods," *J Energy Resour Technol*, vol. 142, no. 10, p. 102106, 2020.

[19] U-Battery, "A differentiated small modular reactor offering providing low cost, low risk, low carbon off-grid energy with a high heat output," https://www.u-battery.com/cdn/uploads/supporting-files/U-Battery_2-pager_handout_final.pdf.

[20] S. T. Revankar, "Nuclear hydrogen production," in *Storage and hybridization of nuclear energy*, Elsevier, 2019, pp. 49–117.

[21] M. J. Moran, H. N. Shapiro, D. D. Boettner, and M. B. Bailey, *Fundamentals of engineering thermodynamics*. John Wiley & Sons, 2010.

[22] R. Augelletti, M. Conti, and M. C. Annesini, “Pressure swing adsorption for biogas upgrading. A new process configuration for the separation of biomethane and carbon dioxide,” *J Clean Prod*, vol. 140, pp. 1390–1398, 2017.

[23] F. Bauer, T. Persson, C. Hulteberg, and D. Tamm, “Biogas upgrading–technology overview, comparison and perspectives for the future,” *Biofuels, Bioproducts and Biorefining*, vol. 7, no. 5, pp. 499–511, 2013.

[24] N. Kohlheb, M. Wluka, A. Bezama, D. Thrän, A. Aurich, and R. A. Müller, “Environmental-economic assessment of the pressure swing adsorption biogas upgrading technology,” *Bioenergy Res*, vol. 14, pp. 901–909, 2021.

[25] D. Saha, H. A. Grappe, A. Chakraborty, and G. Orkoulas, “Postextraction separation, on-board storage, and catalytic conversion of methane in natural gas: a review,” *Chem Rev*, vol. 116, no. 19, pp. 11436–11499, 2016.

[26] A. A. Abd, M. R. Othman, S. Z. Naji, and A. S. Hashim, “Methane enrichment in biogas mixture using pressure swing adsorption: process fundamental and design parameters,” *Materials Today Sustainability*, vol. 11, p. 100063, 2021.

[27] K. Lim, P. J. Evans, and P. Parameswaran, “Long-term performance of a pilot-scale gas-sparged anaerobic membrane bioreactor under ambient temperatures for holistic wastewater treatment,” *Environ Sci Technol*, vol. 53, no. 13, pp. 7347–7354, 2019.

[28] J. Tang *et al.*, “Enhanced methane production coupled with livestock wastewater treatment using anaerobic membrane bioreactor: Performance and membrane filtration properties,” *Bioresour Technol*, vol. 345, p. 126470, 2022.

[29] H. Cheng *et al.*, “Advanced methanogenic performance and fouling mechanism investigation of a high-solid anaerobic membrane bioreactor (AnMBR) for the co-digestion of food waste and sewage sludge,” *Water Res*, vol. 187, p. 116436, 2020.

[30] C. Song, Q. Liu, N. Ji, Y. Kansha, and A. Tsutsumi, “Optimization of steam methane reforming coupled with pressure swing adsorption hydrogen production process by heat integration,” *Appl Energy*, vol. 154, pp. 392–401, 2015.

[31] A. P. Simpson and A. E. Lutz, “Exergy analysis of hydrogen production via steam methane reforming,” *Int J Hydrogen Energy*, vol. 32, no. 18, pp. 4811–4820, 2007.

[32] N. Zhang, X. Chen, B. Chu, C. Cao, Y. Jin, and Y. Cheng, “Catalytic performance of Ni catalyst for steam methane reforming in a micro-channel reactor at high pressure,” *Chemical Engineering and Processing: Process Intensification*, vol. 118, pp. 19–25, 2017.